# CHAPTER V

## GEOCHEMISTRY



As a supplement to petrographic studies, eleven representative rock samples were collected for whole-rock chemical analysis. The first five samples are rocks of the early intermediate-composition lavas consist of two basaltic andesites (sample no.8 and 9), two andesites (no. 6 and 7) and one dacite (no. 5). Three samples (no. 1, 2 and 3) represent rocks of silicic lavas, sampling from a rhyolite lava flow (no. 1 and 2) which rest on the deposit succession of silicic tuffs, and another one from rhyolite lava dome (no. 3). One sample of biotite microgranite (no. 4) which represents the associated intrusive rocks. The last two samples are rocks of late basalt, sampling from the widespread, flat-lying lavas (no. 10), and another one selected from basaltic dyke (no. 11). Locations of these collected samples are shown in Figure 5.1.

All of the analytical works were carried out at the Department of Geology, Faculty of Science, Chulalongkorn University. The standard chemical analyses of major element-oxides and CIPW norms of eleven representative rock samples are demonstrated in Table 5.1.

In order to evaluate the results of the chemical analyses, many diagrams were prepared to show chemical variation and correlation among different kinds of rocks. These diagrams consist

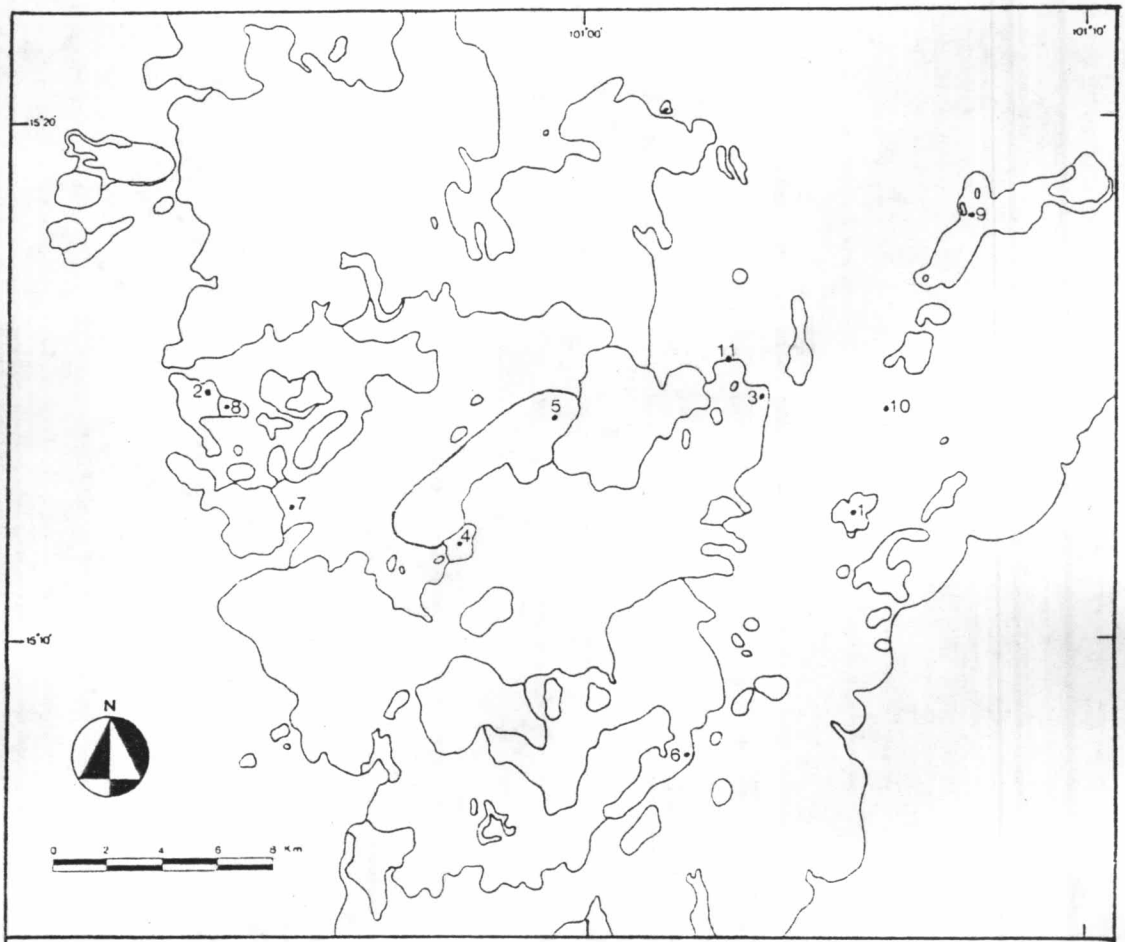


Sample locations.

1,2 From a rhyolite lava flow on the succession of silicic tuffs at Khao Rawang and Khao Tham, respectively.

3 From rhyolite lavas-forming dome.

4 From biotite microgranite.

5 From dacite lava.

6,7 From andesite lavas.

8 From basaltic andesite pyroclast.

9 From basaltic andesite lava.

10 From flat- lying lava flow of late basalt.

11 From basaltic dyke.

Figure 5.1 Sample location map.

Table 5.1 Major element-oxide analyses and CIPW norm.

| | silicic rocks | | | | early intermediate-composition rocks | | | | | late basalt | |
|---|---|---|---|---|---|---|---|---|---|---|---|
| rock type | | | | | | | | | | | |
| sample no. | 1 | 2 | 3 | 4 | 5 | 6 | 7 | 8 | 9 | 10 | 11 |
| **Major element oxides (wt %)** | | | | | | | | | | | |
| $SiO_2$ | 73.50 | 74.49 | 70.10 | 68.25 | 67.00 | 55.50 | 56.80 | 54.79 | 55.40 | 49.80 | 47.50 |
| $TiO_2$ | 0.16 | 0.12 | 0.36 | 0.42 | 0.39 | 0.74 | 0.91 | 0.95 | 1.02 | 1.28 | 1.33 |
| $Al_2O_3$ | 14.95 | 15.40 | 16.81 | 17.04 | 15.79 | 17.27 | 17.58 | 17.58 | 19.03 | 18.29 | 18.93 |
| $Fe_2O_3$ | 1.01 | 0.78 | 1.82 | 2.38 | 2.49 | 4.87 | 5.69 | 4.68 | 4.40 | 6.90 | 7.94 |
| FeO | 0.16 | 0.16 | 0.16 | 0.12 | 0.08 | 0.04 | 0.12 | 0.08 | 0.08 | 0.08 | 0.08 |
| MgO | 0.16 | 0.31 | 0.28 | 0.76 | 0.35 | 3.67 | 3.55 | 2.64 | 2.27 | 4.04 | 3.87 |
| CaO | 0.23 | 0.95 | 0.25 | 0.64 | 0.66 | 3.27 | 6.95 | 5.93 | 4.52 | 7.90 | 7.68 |
| $Na_2O$ | 2.80 | 2.72 | 2.66 | 3.93 | 3.80 | 3.68 | 3.44 | 2.52 | 3.47 | 3.15 | 3.15 |
| $K_2O$ | 4.16 | 4.35 | 4.03 | 3.40 | 4.49 | 1.22 | 1.76 | 3.15 | 3.23 | 1.66 | 1.50 |
| $P_2O_5$ | 0.01 | 0.06 | 0.05 | 0.17 | 0.07 | 0.17 | 0.19 | 0.24 | 0.30 | 0.38 | 0.40 |
| Igloss. | 0.90 | 1.00 | 1.49 | 1.19 | 1.89 | 6.57 | 1.76 | 5.42 | 3.29 | 3.73 | 5.50 |
| Total | 98.04 | 99.67 | 98.01 | 98.30 | 97.01 | 97.02 | 98.75 | 97.98 | 97.01 | 97.21 | 97.97 |
| **CIPW norms** | | | | | | | | | | | |
| Q | 41.79 | 41.69 | 39.78 | 31.26 | 27.31 | 19.28 | 12.65 | 13.20 | 11.35 | 5.79 | 3.10 |
| C | 5.61 | 5.93 | 8.02 | 6.32 | 3.83 | 4.82 | - | - | 2.48 | - | - |
| Or | 25.30 | 26.05 | 24.67 | 20.69 | 27.89 | 7.97 | 10.72 | 20.11 | 20.36 | 10.49 | 9.59 |
| Ab | 24.39 | 23.32 | 23.32 | 34.24 | 33.80 | 34.43 | 30.01 | 23.03 | 31.33 | 28.51 | 28.85 |
| An | 1.11 | 1.01 | 0.95 | 2.13 | 2.96 | 16.71 | 28.18 | 29.55 | 21.83 | 33.02 | 35.81 |
| Di | - | - | - | - | - | - | 2.57 | - | - | 1.41 | - |
| Hy | 0.41 | 0.78 | 0.72 | 1.95 | 0.92 | 10.10 | 7.92 | 7.10 | 6.03 | 10.11 | 10.43 |
| Mt | 5.35 | 0.17 | - | - | - | - | - | - | - | - | - |
| Il | 0.31 | 0.23 | 0.35 | 0.26 | 0.18 | 0.09 | 0.26 | 0.18 | 0.18 | 0.18 | 0.18 |
| Hm | 1.00 | 0.67 | 1.89 | 2.45 | 2.62 | 5.38 | 5.87 | 5.06 | 4.69 | 7.38 | 8.59 |
| Tn | - | - | - | - | - | - | 1.96 | 0.38 | - | 3.13 | 1.83 |
| Ru | - | - | 0.19 | 0.29 | 0.32 | 0.77 | - | 0.78 | 0.99 | - | 0.59 |
| Ap | 0.02 | 0.14 | 0.12 | 0.41 | 0.17 | 0.43 | 0.45 | 0.60 | 0.74 | 0.94 | 1.00 |

of quartz-alkali feldspar-plagioclase (QAP) triangular diagram, $Na_2O + K_2O$ vs $SiO_2$ diagram, $SiO_2$ variation diagrams, $Na_2O + K_2O$, CaO vs solidification index (SI) diagram, AFM ($A = Na_2O + K_2O$, $F = FeO + 0.9Fe_2O_3$, $M = MgO$) triangular diagram, alkali-silica diagram, and alkalinity ratio variation diagram.

Most of the volcanic rocks in the volcanic field, modal mineral content cannot be accurately determined because their textures are mostly of microcystalline, cryptocrystalline or glassy. The classification and nomenclature of these volcanic rocks are therefore based solely on their chemical compositions. Normative quartz, potash feldspar and plagioclase calculated from major oxides of these rocks are plotted in QAP triangular diagram (Figure 5.2) as suggested by IUGS Subcommission (Streckeisen, 1979). Supplementary method for classification of volcanic rocks by plotting $Na_2O + K_2O$ vs $SiO_2$ in a pentagon diagram (Figure 5.3) proposed by Cox et al. (1979) is also used in order to compare their outcomes. Both Figures 5.2 and 5.3 show that the majorities of rock classifications are coincident. It is clearly shown from both figures that volcanic rocks of the Lam Narai volcanic field range in composition from basalt to rhyolite. However, compositions of three volcanic groups of the Lam Narai volcanic field; the early intermediate-composition rocks, silicic rocks (included silicic tuffs and associated microgranite) and late basaltic rock, are relatively separated from each others. There is only one sample of the early intermediate rocks (no. 5) set in the field of rhyolitic composition.

Variation diagram of the major element-oxides plotted against silica oxide is shown in Figure 5.4. It clearly presents that

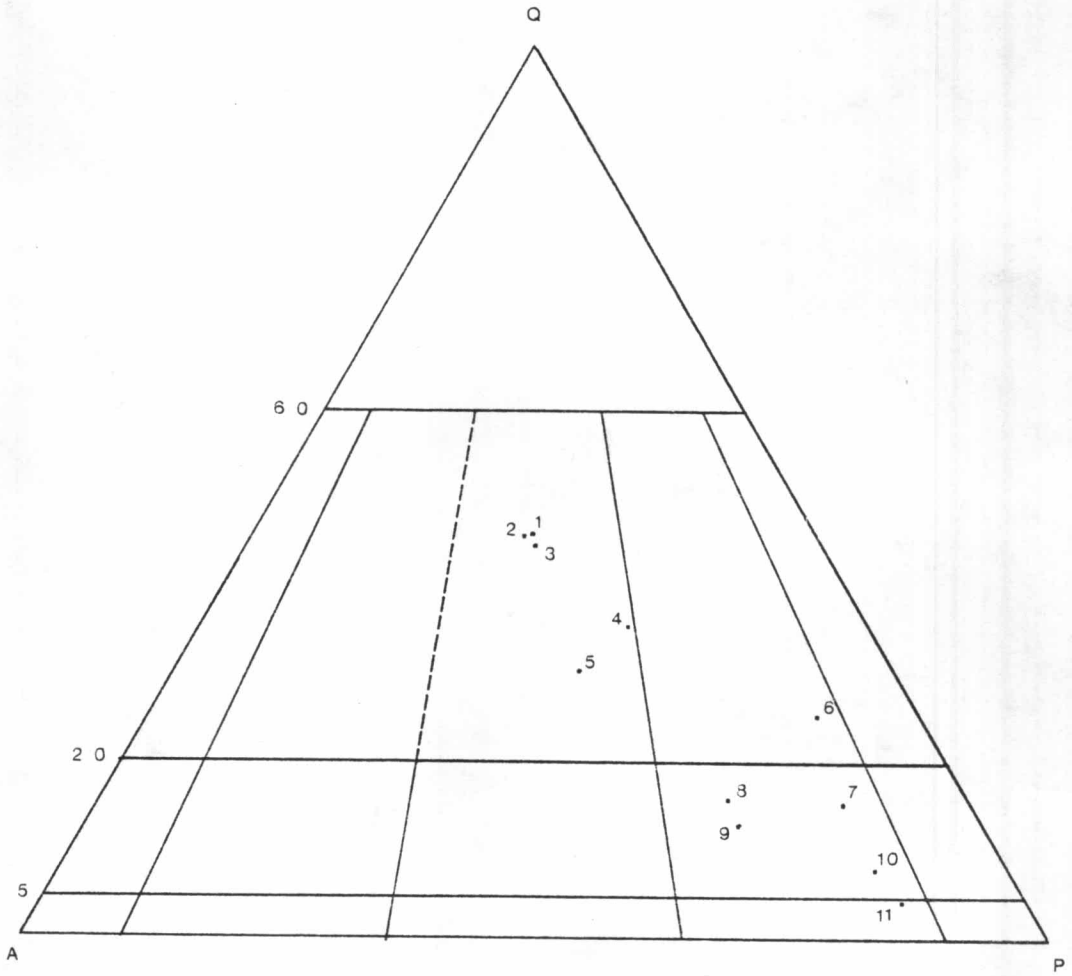


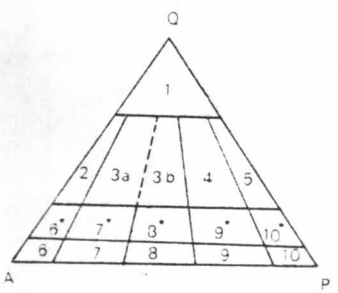


Root names

2 alkali (-feldspar) rhyolite

3a, 3b rhyolite

4, 5 dacite

6* quartz-alkaline (-feldspar) trachyte

6 alkali (-feldspar) trachyte

7* quartz trachyte

7 trachyte

8* quartz latite

8 latite

9, 10 andesite basalt

Figure 5.2 Recommended names of volcanic rocks and their fields in QAP diagram (Streckeisen, 1979).

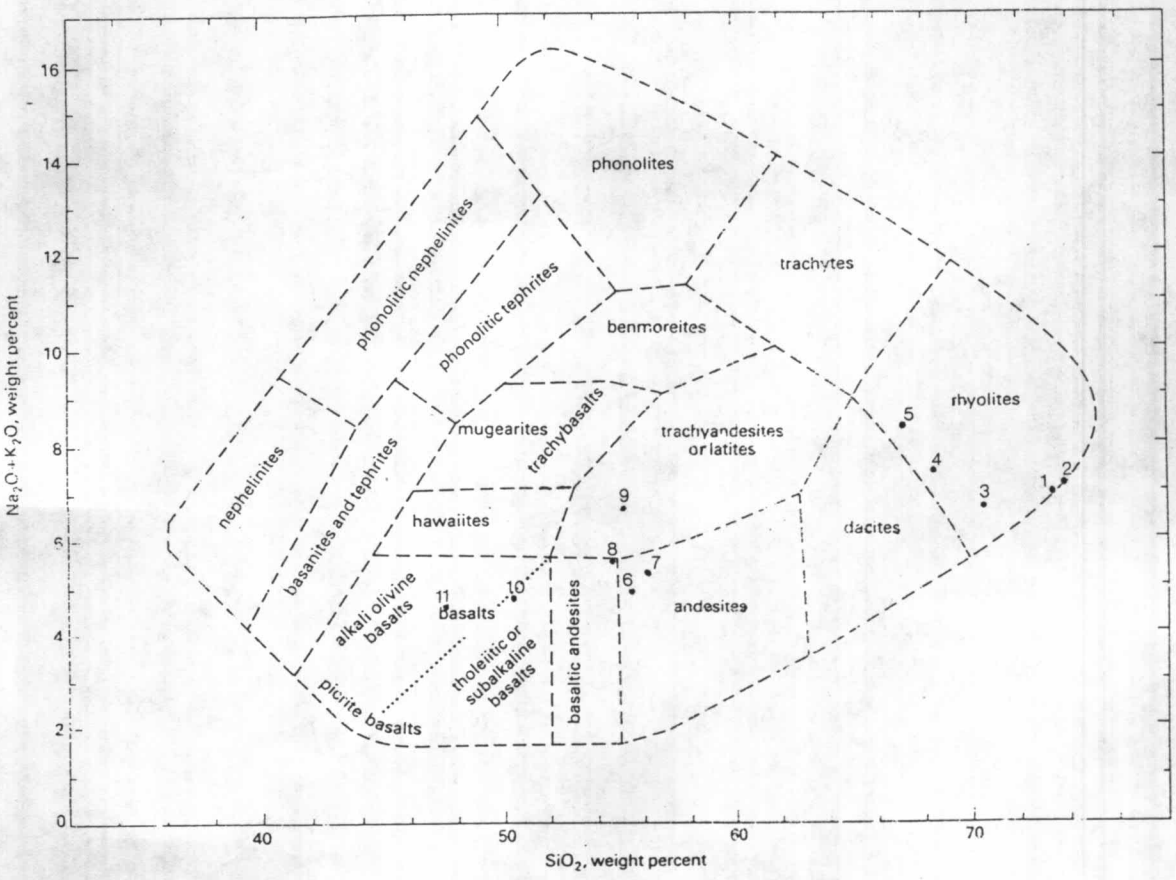


Figure 5.3 Plots of $Na_2O$ + $K_2O$ against $SiO_2$ of the volcanic and associated intrusive rocks in the Lam Narai volcanic field. Nomenclature and boundaries of volcanic rocks are proposed by Cox et al. (1979).

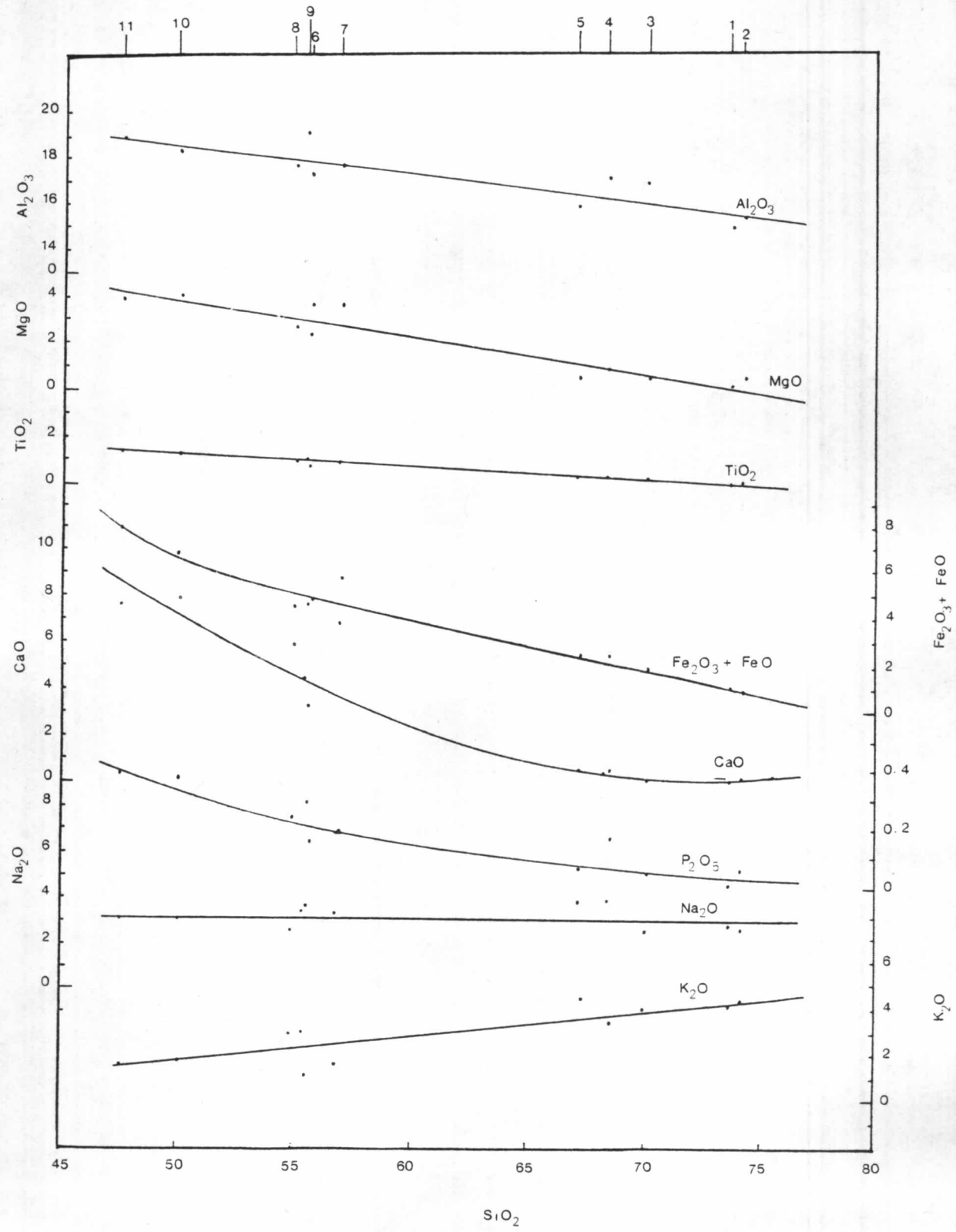


Figure5.4 Variation of major element-oxides against silica-oxide for volcanic and related intrusive rocks of the volcanic field.

variations of most of the major element-oxides are decreasing or increasing relatively smooth in response to the increasing of $SiO_2$ content. Veerote Daorerk (1972) suggested that the smooth variations indicate the strong genetic relationship between the rocks with the complete differentiation from a basic end member to an acid end member. However, the clear separation of each volcanic group of the volcanic field basing on $SiO_2$ content is likely to suggest that the origin of these volcanic rocks did not generate from the continuous differentiation. The sudden decrease of $Fe_2O$ + FeO curve from late basaltic rocks (no. 10 and 11) to the early intermediate-composition rocks (no. 6, 7, 8 and 9) may also suggest the origin of the late basaltic rocks did not differentiate from the origin of the early intermediate-composition rocks and silicic rocks.

The discontinuity of $Fe_2O$ + FeO curve is also reflected in the AFM triangular diagram (Figure 5.5). The olivine basalt from flat-lying basaltic lava (no. 10) and basaltic dyke (no. 11) lie in the trend of alkali-series. While the early intermediate-composition rocks and silicic rocks show the differentiate trend of typically calc-alkali series. This trend is nearly perpendicular to MgO-FeO sideline. It starts up near the MgO-FeO sideline with moderate iron concentration of the early intermediate-composition rocks. The FeO and MgO decrease gradually to the later stage silicic rocks with contemporaneous increase in the $Na_2O$ + $K_2O$ contents.

Figure 5.6 shows the alkalinity ratio of all rock samples plotted against their $SiO_2$ contents. The majority of samples fall in a typical calc-alkaline field affinity, except two samples of late basaltic rocks become more alkaline with decreasing $SiO_2$.

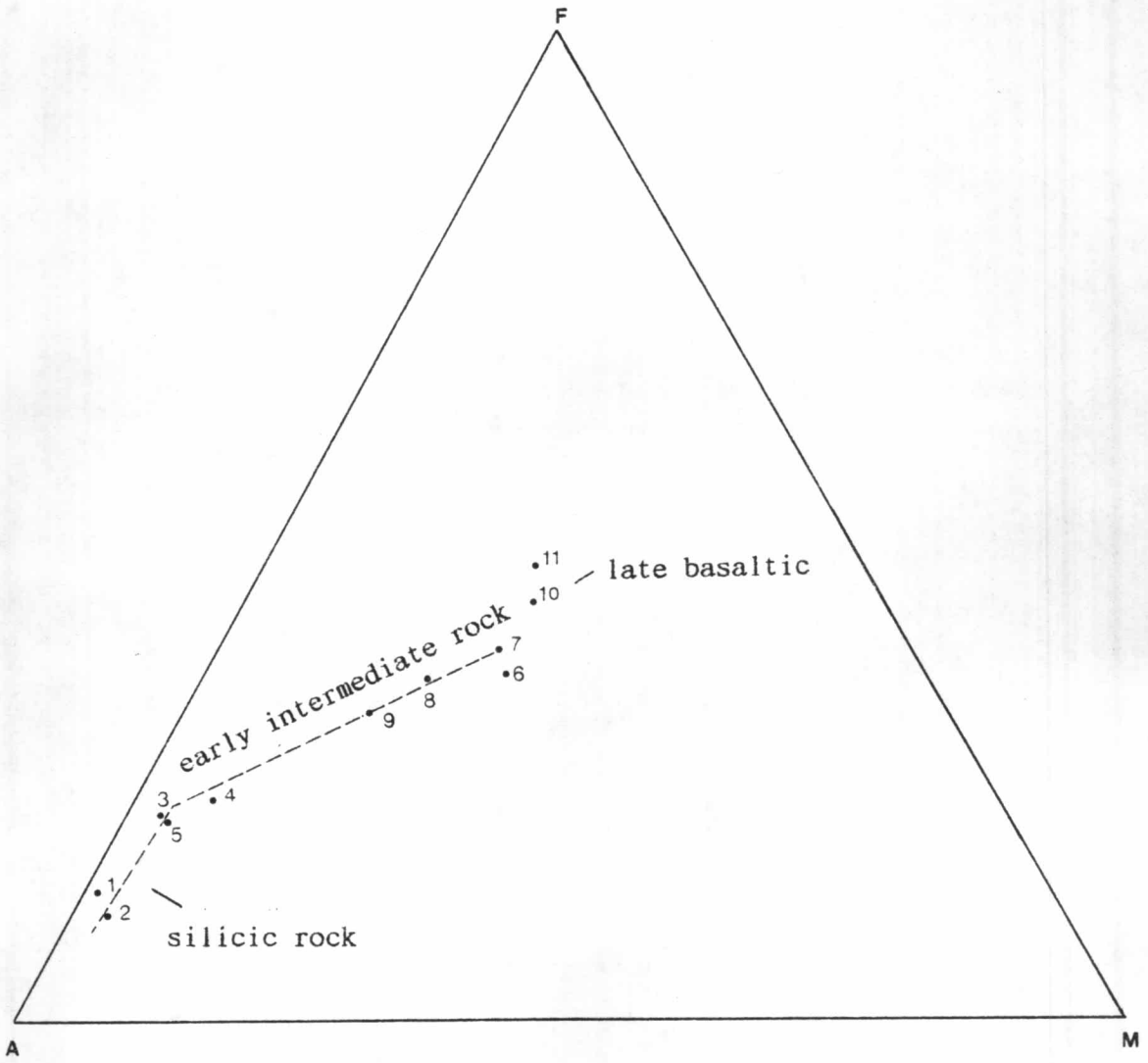


Figure5.5 AFM diagram of volcanic and associated intrusive rocks of the Lam Narai volcanic field; A = $Na_2O + K_2O$, F = $FeO + 0.9Fe_2O_3$, M = MgO (Miyashiro, 1974).

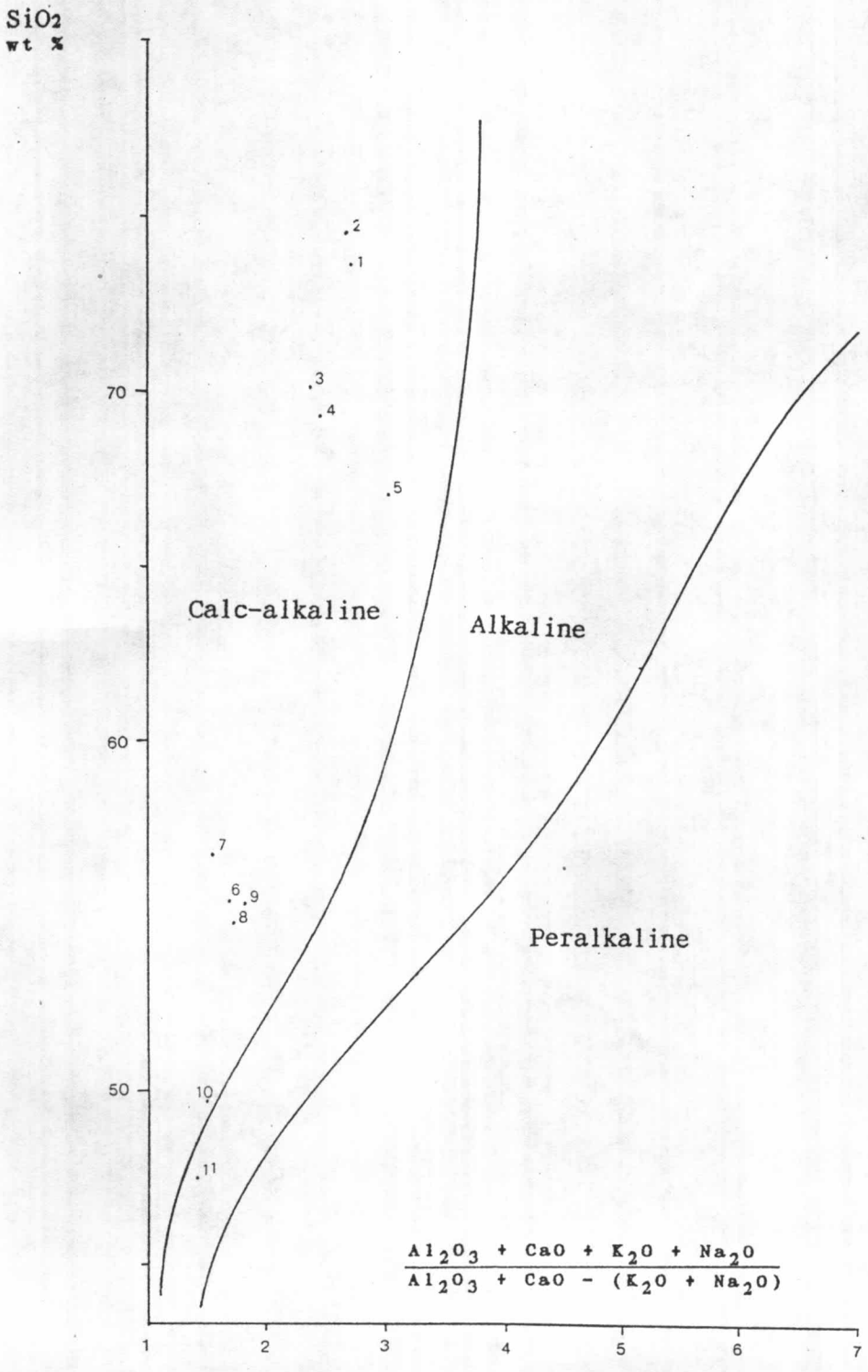


Figure 5.6 Alkalinity ratio variation diagram for rocks of the Lam Narai volcanic field. The alkalinity fields are from Wright (1969, cited in Sheraton and Labonne, 1978).

The volcanic and associated intrusive rocks of the Lam Narai volcanic field are designated to be rocks of calc-alkaline series when using the method of which proposed by Kuno in 1959 (Figures 5.7 and 5.8).

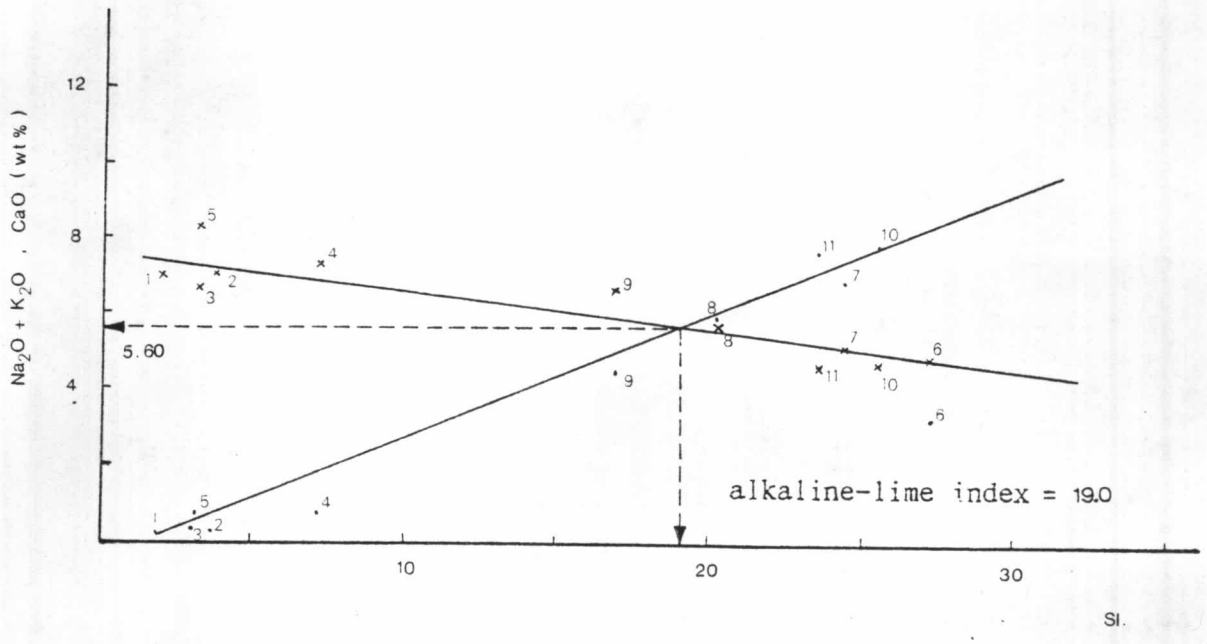


Figure 5.7 Plots of $Na_2O + K_2O$, CaO against solidificaton index (SI) leading to alkaline-lime index of the Lam Narai volcanic field.

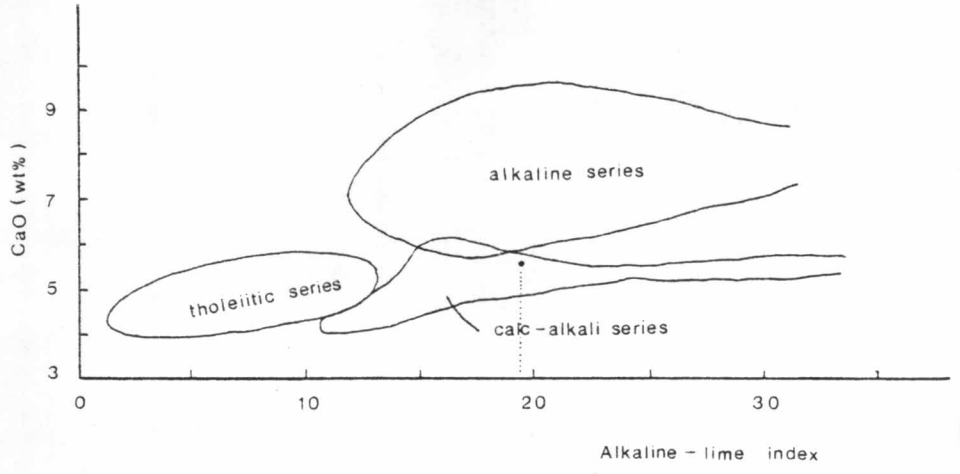


Figure 5.8 Plots of CaO against alkaline-lime index giving a good separation of rocks into tholeiitic, alkaline, and calc-alkaline series (after Kuno, 1959); and showing composition of the Lam Narai volcanic field falling in the boundary of calc-alkaline series.